Experimental and theoretical aspects of the haptotropic rearrangement of diiron and diruthenium carbonyl complexes bound to 4,6,8-trimethylazulene†

Kazuhiro Tsuchiya,[a] Keiko Ideta,[b] Koichi Mogi,[c] Yusuke Sunada[a] and Hideo Nagashima*[a,c]

Received 14th December 2007, Accepted 14th February 2008
First published as an Advance Article on the web 25th March 2008
DOI: 10.1039/b719331a

The haptotropic rearrangement of dinuclear metal carbonyl species on the conjugate π-ligand of (μ_2,η^3:η^5-4,6,8-trimethylazulene)$M_2(CO)_5$ [M = Fe (**3**) and Ru (**4**)] was investigated in detail both experimentally and theoretically. The complexes, **3** and **4**, were synthesized and characterized by spectroscopy and crystallography. The spin saturation transfer technique of ^{1}H NMR was used to measure the rate constant k of the haptotropic isomerization between the two enantiomers of **3** and **4**, from which thermodynamic parameters were determined: (**3**; $\Delta S^{\ddagger} = -7 \pm 1$ cal K^{-1} mol^{-1}, $\Delta H^{\ddagger} = 22 \pm 1$ cal mol^{-1}, $\Delta G^{\ddagger}_{373} = 25 \pm 1$ cal mol^{-1}), (**4**; $\Delta S^{\ddagger} = 7 \pm 1$ cal K^{-1} mol^{-1}, $\Delta H^{\ddagger} = 25 \pm 1$ cal mol^{-1}, $\Delta G^{\ddagger}_{373} = 23 \pm 1$ cal mol^{-1}). DFT calculations (the B3LYP, B1B95 and PBE1PBE methods) were also carried out using the CEP-31G and cc-pVDZ as the basis set of the transition metal and other elements, respectively, by which both ground state and transition state structures were optimized for the haptotropic rearrangement of **3** and **4**. The potential energy surface for these reactions suggests that the reaction involves the conversion of the coordination mode from μ_2,η^3,η^5- (ground state) to μ_2,η^1,η^5- (transition state). Mechanistic consideration, in particular that of differences in transition states between the diiron and diruthenium complexes, is also described.

Introduction

Hapticity change of conjugated π-ligands increases flexibility of their coordination modes, leading to high reactivity toward ligand exchange processes and other organometallic reactions.[1] The haptotropic rearrangement, which is one of the interesting outcomes of the hapticity change, is slipping of a transition metal fragment from one coordination site to the other with total electron count remaining intact on a polyaromatic hydrocarbon or cyclic polyene ligand.[2,3] A number of studies on the haptotropic rearrangement in mononuclear transition metal compounds bearing such ligands have been undertaken experimentally[4] and theoretically.[5] Among them, reversible site exchange of (η^6-naphthalene)$Cr(CO)_3$ and its derivatives and reaction from (η^5-indenyl)$Cr(CO)_3$Me to (η^6-methylindene)$Cr(CO)_3$ are one of the well-investigated class of the haptotropic rearrangement, in which mechanisms involving slipping of $Cr(CO)_3$ species on the conjugated π-systems are proposed from kinetic analysis and DFT calculations.[6] Discussion on the transition state was made for (η^6-naphthalene)$Cr(CO)_3$; the interconversion between two haptotropic isomers takes place through a trimethylenemethane-like (η^4-naphthalene)$Cr(CO)_3$ as the transition state. In other words, migration of the $Cr(CO)_3$ species from one benzene ring to the other results in hapticity change of the naphthalene ring from $\eta^6 \leftrightarrow \eta^4 \leftrightarrow \eta^6$, and the transition state is a coordinatively unsaturated species bearing 16 valence electrons.

In contrast to the relatively well-studied mononuclear complexes, only a few reports have been published on the rearrangement of the dinuclear systems.[7–9] Diiron and diruthenium carbonyl complexes (μ_2,η^3,η^5-guaiazulene)$M_2(CO)_5$ [M = Fe (**1**) and Ru (**2**)] have two haptotropic isomers, **1A** and **1B** or **2A** and **2B**. Studies on the CO scrambling processes of these complexes were carried out by Cotton *et al.* in 1977, in which the authors briefly mentioned that thermal interconversion between the haptotropic isomers concomitantly took place.[7a] In our previous papers, we reported studies on the haptotropic rearrangement of two dinuclear metal carbonyls bound to guaiazulene, **1** and **2**, in which two haptotropic isomers of each complex were isolated and characterized, and the thermal and photochemical interconversions of the isomers were investigated as shown in Scheme 1.[7b–d] The reactions are not only unique for their photo-switch like behavior, in which the isomer ratios in the thermal equilibrium are substantially different from those in photostatic states.[8] The mechanism of the photochemical haptotropic rearrangement of these dinuclear complexes requires further investigation on the exited states. In contrast, that of thermal interconversion is expected to be similar to that of the haptotropic rearrangement of mononuclear complexes. Thus, a possible scheme is drawn as Scheme 2, in which the $M_2(CO)_5$ species migrates from one η^5,η^3-coordination site to the other *via* the coordinatively unsaturated η^5,η^1-transition state whilst retaining the metal–metal bond. This scheme is in accord with experimental results reported in our previous papers. For

[a]*Division of Applied Molecular Chemistry of Institute for Material Chemistry and Engineering, Kyushu University, Kasuga, Fukuoka, 816-8580, Japan. E-mail: nagasima@cm.kyushu-u.ac.jp*
[b]*Analytical Center of Institute for Material Chemistry and Engineering, Kyushu University, Kasuga, Fukuoka, 816-8580, Japan*
[c]*Department of Molecular and Materials Science, Graduate School of Engineering Sciences, Kyushu University, Kasuga, Fukuoka, 816-8580, Japan*

† Electronic supplementary information (ESI) available: SST data and Cartesian coordinates of ground and transition state structures of **3** and **4** by DFT calculations. CCDC reference numbers 284581 and 284582. For ESI and crystallographic data in CIF or other electronic format see DOI: 10.1039/b719331a

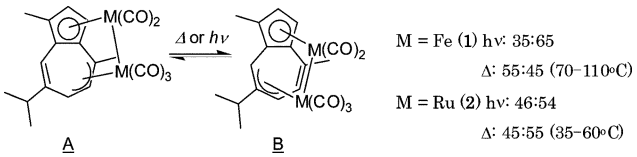

Scheme 1

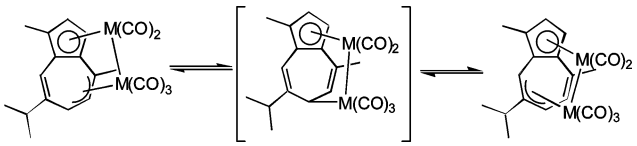

Scheme 2

example, an alternative mechanism involving CO dissociation, *i.e.* the pathway from one (μ_2,η^3,η^5-guaiazulene)$M_2(CO)_5$ isomer to the other *via* the (μ_2,η^3,η^5-guaiazulene)$M_2(CO)_4$ intermediate, can be excluded by the impossible trapping of the intermediate by other ligands.

The aim of this paper is to get evidence suggesting the mechanism shown in Scheme 2 is rational. For this, we carried out the following studies. First is the experimental study, in which the C_{2v}-symmetric 2,4,6-trimethylazulene is used as the ligand of $M_2(CO)_5$ species. As illustrated in Scheme 3, the haptotropic rearrangement between the two enantiomers of **3** and **4** proceeds through the symmetric structure shown as **X**. We carried out synthesis, structure determination, and spectroscopic assignments of compounds **3** (M = Fe) and **4** (M = Ru). Since the two possible haptotropic isomers are identical, the haptotropic rearrangement was detected by spin saturation transfer (SST).[10,11] Thermodynamic parameters are calculated from the SST studies of **3** and **4**. The second part of this study is DFT calculations to analyze the reaction pathway, in particular, whether the mechanism shown in Scheme 3 is theoretically valid. Three functionals are subjected to the studies to calculate structures of **3** and **4**, and used in search for transition states. Comparison of the former with the structures determined by crystallography provides a solid basis to discuss the possible transition states.

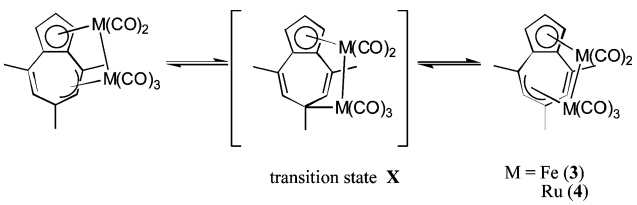

Scheme 3

Results and discussion

Synthesis and characterization of (μ_2,η^3:η^5-4,6,8-trimethylazulene)$Fe_2(CO)_5$ (3) and (μ_2,η^3:η^5-4,6,8-trimethylazulene)$Ru_2(CO)_5$ (4)

The synthesis of **3** was performed by a procedure similar to that used for preparation of (μ_2,η^3:η^5-guaiazulene)$Fe_2(CO)_5$[7] and (μ_2,η^3:η^5-aceanthrylene)$Fe_2(CO)_5$.[8] Thus, a xylene solution of 4,6,8-trimethylazulene and an excess amount of $Fe(CO)_5$ was heated under reflux with stirring for 2 days to afford (μ_2,η^3:η^5-4,6,8-trimethylazulene)$Fe_2(CO)_5$ in 37% yield.

The synthesis of (μ_2,η^3:η^5-4,6,8-trimethylazulene)$Ru_2(CO)_5$ was carried out according to a method reported previously;[12] 4,6,8-trimethylazulene was treated with $Ru_3(CO)_{12}$ in heptane under reflux for 5 h to form a mixture of **4**, (μ_2,η^3:η^5-4,6,8-trimethylazulene)$Ru_3(CO)_7$ and (μ_2,η^3:η^5-4,6,8-trimethylazulene)$Ru_4(CO)_9$, from which **4** was isolated by silica gel column chromatography. The spectral data (^{1}H and ^{13}C NMR in xylene-d_{10} and IR in KBr) of **3** and **4** are listed in Table 3. For the SST experiments described below, all of the ^{1}H resonances are carefully assigned with the aid of NOE experiments in ^{1}H NMR, except for the signals due to the methyl groups.

Structural determinations of **3** and **4** were performed by X-ray crystallography. ORTEP drawings are illustrated in Fig. 1 while crystallographic data, and representative bond distances are summarized in Tables 1 and 2, respectively. The diiron or diruthenium moiety was bound to eight carbons in the azulene ligand with a Cp and a π-allyl coordination mode. Two CO ligands were bonded to one of the metals, whereas the remaining three were bound to the other. These structures are in accord with those deduced from the spectroscopic data described above. The difference of the metal, *i.e.*, Ru or Fe, has some influence on the structure, in particular the metal–metal bond distance; that of **4** [Ru1–Ru2 2.8660(4)] is longer than that of **3** [Fe1–Fe2 2.7820(4)]. The metal–carbon distances are also dependent on the metal; metal–carbon bond distances of **4** [Ru–C_{Cp} 2.232(3)–2.258(3) Å; Ru–C_{allyl} 2.202(3)–2.335(3) Å] are longer than **3** [Fe–C_{Cp} 2.088(2)– 2.113(2) Å; Fe– C_{allyl}; 2.068(2)–2.234(2)] by 0.12 Å. These results are due to that the difference of the atom radius of Fe and Ru induce differences in planarity of the azulene ligand; the azulene ligand is no longer planar by coordination to the diiron or diruthenium moiety, but the distortion is more significant in the iron complex than in the diruthenium homologue.

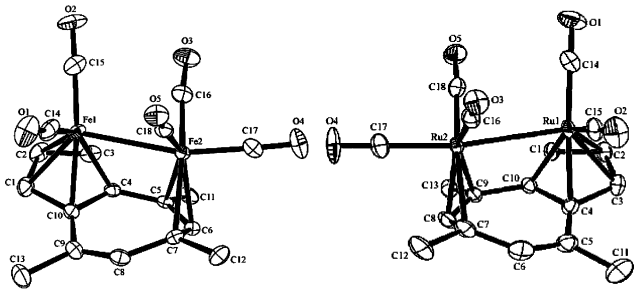

Fig. 1 ORTEP drawings of dinuclear carbonyl complexes, **3** (left) and **4** (right) (50% thermal probability ellipsoids).

Spin-saturation transfer studies

Since the two haptotropic isomers of **3** or **4** are identical, we looked to obtain evidence for the haptotropic rearrangement of the trimethylazulene complexes **3** and **4** by analyses of their fluxional behavior using the variable-temperature NMR technique. From the rearrangement temperature of **1** and **2**, haptotropic interconversions of **3** and **4** were expected to occur above 70 °C. Line broadening analysis around this temperature

Table 1 Crystal data and parameters for **3** and **4**

	3	**4**
Empirical formula	$C_{18}H_{14}Fe_2O_5$	$C_{18}H_{14}Ru_2O_5$
M_r	422.00	512.45
Crystal color, habit	Brown, block	Yellow, block
Crystal dimensions/mm	0.13 × 0.13 × 0.09	0.14 × 0.13 × 0.07
Crystal system	Monoclinic	Monoclinic
Space group	$P2_1/n$ (no. 14)	$P2_1/c$ (no. 14)
Lattice type	Primitive	Primitive
a/Å	11.142(2)	9.262(7)
b/Å	13.089(2)	14.046(10)
c/Å	11.895(2)	13.427(10)
β/°	106.3366(8)	96.721(6)
V/Å^3	1664.7(5)	1734.8(23)
Z	4	4
D_c/g cm^{-3}	1.684	1.962
F_{000}	856.00	1000.00
μ(Mo-Kα)/cm^{-1}	17.66	17.66
$2\theta_{max}$/°	55.0	55.0
λ(Mo-Kα)/Å	0.71070	0.71070
R_{int}	0.030	0.051
No. rflns measd	13181	20376
No. unique rflns	3727	3951
Reflection/param. ratio	15.50	16.43
$R1$ (all)	0.035	0.035
$R1$ ($I > 2\sigma(I)$)	0.027	0.027
$wR2$ (all)	0.074	0.075
GOF	1.000	1.002
Max. shift/error in final cycle	0.000	0.000
$\Delta\rho_{max}$/e Å^{-3}	0.65	1.19
$\Delta\rho_{min}$/e Å^{-3}	−0.28	−1.04

Table 2 Selected bond lengths (Å) for **3** and **4** (X-ray crystal data)

3		**4**	
Fe1–Fe2	2.7820(4)	Ru1–Ru2	2.8660(4)
Fe1–C1	2.107(2)	Ru1–C1	2.247(3)
Fe1–C2	2.104(2)	Ru1–C2	2.258(3)
Fe1–C3	2.090(2)	Ru1–C3	2.251(3)
Fe1–C4	2.113(2)	Ru1–C4	2.232(3)
Fe1–C10	2.088(2)	Ru1–C10	2.278(3)
Fe2–C5	2.145(2)	Ru2–C7	2.335(3)
Fe2–C6	2.068(2)	Ru2–C8	2.202(3)
Fe2–C7	2.234(2)	Ru2–C9	2.275(3)
C4–C5	1.453(3)	C4–C5	1.467(4)
C5–C6	1.408(3)	C5–C6	1.341(4)
C6–C7	1.421(3)	C6–C7	1.480(4)
C7–C8	1.470(3)	C7–C8	1.421(4)
C8–C9	1.343(3)	C8–C9	1.411(3)
C9–C10	1.465(3)	C9–C10	1.467(4)

is one of the methods; however, variable-temperature ^{1}H NMR studies of **3** and **4** showed that no line broadening was observed from room temperature to 130 °C. This suggests that haptotropic rearrangement of **3** and **4** is too slow to detect the NMR line-broadening method, and the SST experiment would instead be useful for its detection. It should be noted that there exists another fluxional process, the site exchange of the CO ligands. Five ν_{CO} absorptions due to the five CO ligands were seen in the IR spectra of **3** and **4** at room temperature. In contrast, five ^{13}C resonances due to the five CO ligands were observed only below −50 °C in CD_2Cl_2, and coalescence of a part of the signals was seen above this temperature. At the temperature of which the SST experiments are performed (80–138 °C), the CO exchange processes are too rapid to detect in an NMR time scale, and have no influence for ^{1}H resonances on the 4,6,8-trimethylazulene ligand in **3** and **4**.

The SST studies of **3** and **4** were carried out in the temperature range of 349 to 402 K (Fig. 2). Since a proton resonance due to H3 appeared independently at a higher field than the others in xylene-d_{10}, we decided to irradiate this signal and see the change of intensity of the resonance due to H1. The spin–lattice relaxation time of H1 $\{T_1(H1)\}$ was determined by the standard inversion recovery method as the average of ten measurements at 388, 393, 398, 402, 407 and 411 K for complex **3**, and 353, 358, 363, 368, 373 and 378 K for complex **4**. Then, we measured the spectrum at each of these temperatures with the spin decoupler applied on the resonance due to H3 for a period of at least $5T_1$ before the probe pulse. As we expected, peak intensity of H1 was apparently decreased in raising the probe temperature in each experiments; this clearly the evidence for the haptotropic rearrangement.

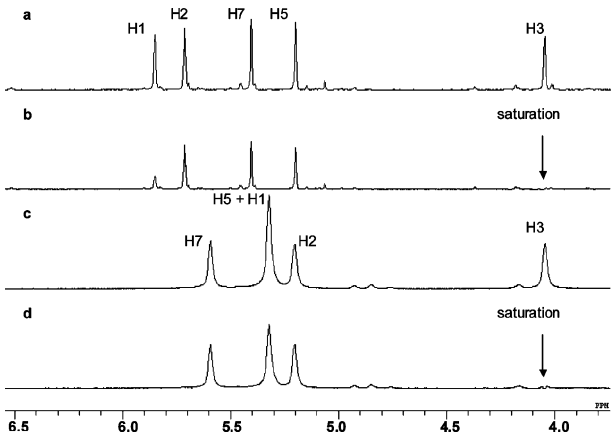

Fig. 2 SST measurements of complexes **3** and **4**. (a) Complex **4** in xylene-d_{10} at 100 °C without saturation; (b) the same as (a) with saturation of H3; (c) complex **3** in xylene-d_{10} at 130 °C without saturation; (d) the same as (c) with saturation of H3.

The rate of rearrangement was estimated from change of the integral value of the peak due to H1. The I_0/I_f, where I_0 is the initial intensity of H1 while I_f is the final intensity, was calculated, from which the exchange rate k was determined according to the equation, $I_0/I_f = \{T_1(H1)\}^{-1}/[k + \{T_1(H1)\}^{-1}]$.

$$k = \frac{1}{T_{1(H1)}}\left(\frac{I_{0(H1)}}{I_{f(H1)}} - 1\right) \quad (1)$$

The T_1(H1), I_0/I_f and k at each temperature are listed in Table 3. For the exchange rate k, ten measurements were performed at each temperature, and the average was adopted to an Eyring plot of $\ln(k/T)$ *vs.* $1000/T$ as shown in Fig. 3. The best-fit line drawn from a least-squares analysis of the plot provided the enthalpy and entropy of activation from the slope and the intercept, respectively. The calculated $\Delta G^{\ddagger}_{373}$, $\Delta H^{\ddagger}$ and $\Delta S^{\ddagger}$ for the rearrangement of **3** and **4** are listed in Table 4, which contains those for the reaction of **1** and **2** determined by kinetics in our earlier studies. The $\Delta G^{\ddagger}_{373}$ values in the rearrangement of **1**, **2**, **3** and **4** are roughly the same, when we consider the experimental errors and the differences on the substituent of the azulene ligands (**1** and **2**; guaiazulene, **3** and **4**; 4,6,8-trimethylazulene). The value of 20–30 kcal mol^{-1}

Table 3 T_1(H1), I_0/I_f, and k for **3** (Fe) and **4** (Ru)

Complex	T^a/K	$T_{1(H1)}{}^b$/s	$I_{f(H1)}/I_{0(H1)}{}^c$	k^d
3	388	7.12 (0.20)	0.738 (0.02)	−8.94 (0.35)
	393	7.30 (0.13)	0.643 (0.03)	−8.53 (0.43)
	398	7.01 (0.08)	0.570 (0.01)	−8.19 (0.17)
	402	6.98 (0.19)	0.513 (0.01)	−7.97 (0.32)
	407	5.71 (0.10)	0.492 (0.01)	−7.70 (0.30)
	411	6.22 (0.05)	0.401 (0.02)	−7.42 (0.25)
4	353	6.54 (0.14)	0.84 (0.01)	−9.39 (0.46)
	358	7.32 (0.46)	0.74 (0.03)	−8.90 (0.84)
	363	7.45 (0.08)	0.62 (0.01)	−8.38 (0.19)
	368	7.32 (0.11)	0.52 (0.004)	−8.00 (0.21)
	373	7.12 (0.09)	0.40 (0.002)	−7.47 (0.14)
	378	7.44 (0.78)	0.33 (0.01)	−7.18 (0.87)

[a] The temperature contains errors of 0.5 K. [b] Average of ten measurements. The figures in parentheses are standard deviations. [c] The figures in parentheses are standard deviations. [d] Calculated from eqn (1). The figures in parentheses are standard deviations.

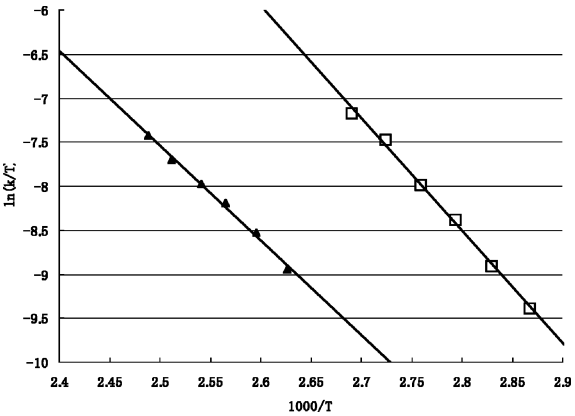

Fig. 3 Eyring plot for the haptotropic rearrangement of **3** (▲) and **4** (□).

Table 4 Thermodynamic parameters for the rearrangements of **1**–**4**

	1[a]	**2**[a]	**3**[b]	**4**[b]
$\Delta G^{\ddagger}_{373}$/kcal mol^{-1}	28 ± 1	25 ± 1	25 ± 1	23 ± 1
$\Delta H^{\ddagger}$/kcal mol^{-1}	23 ± 2	26 ± 2	22 ± 1	25 ± 1
$\Delta S^{\ddagger}$/cal mol^{-1} K^{-1}	−15 ± 5	1 ± 2	−7 ± 1	7 ± 1

[a] Determined by kinetics.[7b,c] [b] Determined by the SST experiments. Experimental errors were determined by the least squares of the Eyring plot. Note that the T_1 value, which is the basis to calculate k, contains ~10% experimental errors.

are similar to those seen in the haptotropic rearrangement of mononuclear metal carbonyls bound to arene ligands. The $\Delta S^{\ddagger}$ values are negative in the diiron complexes **1** and **3**, whereas they are positive in the diruthenium complexes, **2** and **4**. These results show little difference in the thermodynamic parameters between the haptotropic rearrangement of **1** or **2** and those of **3** or **4**, respectively, indicating the thermal haptotropic rearrangements of the trimethylazulene complexes proceed through similar reaction pathways to those of the guaiazulene complexes.

DFT calculations

As described in the Introduction, the haptotropic rearrangement is generally explained by successive hapticity change, namely, slipping of the metal species on the conjugated π-electrons. Based on the assumption that symmetric transition states **X** are involved in the reaction mechanisms (Scheme 4), we carried out DFT calculations (the B3LYP method)[13] using the CEP-31G[14] and cc-pVDZ[15] as the basis set of the transition metal and other elements, respectively. B3LYP functional is the most successful model among the standard density functional approximations, which includes three empirical parameters optimized by a best fit to atomization energies, being used for many theoretical studies on the organometallic reactions.[16]

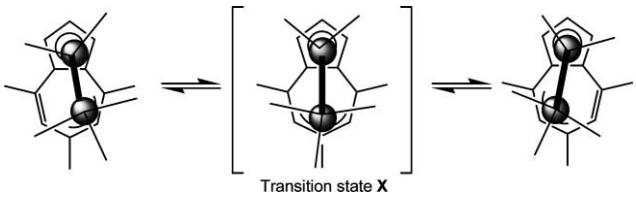

Scheme 4

Geometrical optimization of ground state structures of **3** and **4** provided the molecular structures close to those determined by crystallography; representative bond distances are listed in Table 5. Although the metal–metal bond and metal–carbon distances determined by the B3LYP method are slightly longer than those observed by crystallography, similarities in the structures suggests that the calculation is accurate enough to realize the experimentally proved structures. In both the crystal structures and the theoretically optimized structures, the metal–metal bond length is Fe–Fe < Ru–Ru, which can typically be seen on the average bond distances between M(1) and η^5-coordinated carbons and between M(2) and η^3-coordinated carbons of the azulene ligand (M = Fe, Ru). Results of investigation of the potential energy surface are summarized in Fig. 4. There are two reaction pathways in both of the Fe and Ru complexes. The main pathway is the interconversion between the two enantiomers with retention of the metal–metal bond. The reaction takes place through a C_s-symmetric transition state, Fe[TS] or Ru[TS], with the activation energy of 27.1 (M = Fe) or 19.0 (M = Ru) kcal mol^{-1}. The secondary pathway involves metal–metal bond cleavage prior to the isomerization, proceeding through transition states having a bridging carbonyl, Fe[TS(a)] and Ru[MS]. The activation energy of the secondary pathways is 17.9 and 23.6 kcal mol^{-1} higher than that of the main pathways for the diiron and diruthenium complex, respectively. The probability of the reaction pathways (main : secondary) at 398 K is nearly 100 : 0 for both the Fe and Ru complexes, suggesting that only the main pathway is important for further discussion.

With the assumption that the rearrangement proceeds through the main pathway, we next carried out the DFT calculations using other functionals, the one-parameterized hybrid functionals, B1B95[17] and PBE1PBE.[18] Both of the calculations provided the ground state structures for diiron and diruthenium complexes similar to those obtained by the B3LYP method. To our surprise, however, the bond distances calculated with the one-parameterized hybrid functionals are closer to those obtained

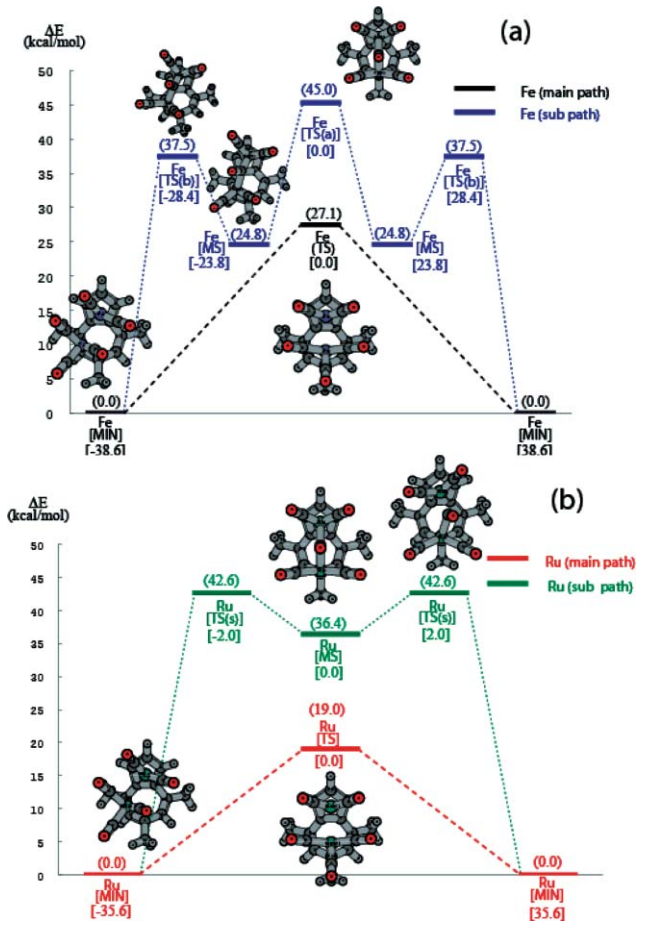

Fig. 4 Potential energy surface of haptropic rearrangement: (a) diiron complex **3** and (b) diruthenium complex **4**. The main and secondary reaction pathways are indicated by *black* and *blue* lines, respectively, for (a) diiron complex **3** and *red* and *green* lines, respectively, for (b) diruthenium complex **4**. The minimum, transition state and metastable structures are abbreviated by MIN, TS and MS on these surfaces. The energy differences (kcal mol^{-1}) from the minimum structure for each stationary structure is given in parentheses, and the dihedral angles *D*[C(7)–C(2)–M(1)–M(2)] (°) (M = Fe, Ru, the numbering is shown in Fig. 5) on each stationary structure is given in square brackets.

Table 5 Selected bond lengths (Å) for **3** and **4** by DFT calculation. (ground state)

3 [Fe]				
	Exptl. (X-ray)	B3LYP	B1B95	PBE1PBE
Fe(1)–Fe(2)	2.7820(4)	2.853	2.729	2.765
Fe(1)–C(1)	2.107(2)	2.121	2.069	2.075
Fe(1)–C(2)	2.104(2)	2.124	2.076	2.081
Fe(1)–C(3)	2.090(2)	2.113	2.070	2.076
Fe(1)–C(4)	2.113(2)	2.126	2.090	2.091
Fe(1)–C(10)	2.088(2)	2.112	2.062	2.073
Fe(1)–C_{η^5}	*2.100*	*2.119*	*2.074*	*2.079*
Fe(2)–C(5)	2.145(2)	2.184	2.123	2.130
Fe(2)–C(6)	2.068(2)	2.085	2.044	2.044
Fe(2)–C(7)	2.234(2)	2.264	2.187	2.202
Fe(2)–C_{allyl} (av.)	*2.149*	*2.178*	*2.118*	*2.125*
C(4)–C(5)	1.453(3)	1.462	1.455	1.459
C(5)–C(6)	1.408(3)	1.411	1.405	1.410
C(6)–C(7)	1.421(3)	1.430	1.427	1.429
C(7)–C(8)	1.470(3)	1.473	1.469	1.471
C(8)–C(9)	1.343(3)	1.352	1.345	1.348
C(9)–C(10)	1.465(3)	1.466	1.459	1.461
4 [Ru]				
	Exptl. (X-ray)	B3LYP	B1B95	PBE1PBE
Ru(1)–Ru(2)	2.866(4)	2.971	2.878	2.902
Ru(1)–C(1)	2.247(3)	2.294	2.239	2.251
Ru(1)–C(2)	2.258(3)	2.316	2.254	2.263
Ru(1)–C(3)	2.251(3)	2.307	2.242	2.253
Ru(1)–C(4)	2.232(3)	2.286	2.226	2.241
Ru(1)–C(10)	2.278(3)	2.313	2.267	2.274
Ru(1)–C_{η^5} (av.)	*2.253*	*2.303*	*2.245*	*2.256*
Ru(2)–C(7)	2.335(3)	2.408	2.322	2.341
Ru(2)–C(8)	2.202(3)	2.250	2.200	2.204
Ru(2)–C(9)	2.275(3)	2.367	2.294	2.305
Ru(2)–C_{allyl}	*2.271*	*2.329*	*2.261*	*2.283*
C(4)–C(5)	1.467(4)	1.464	1.459	1.461
C(5)–C(6)	1.341(5)	1.355	1.347	1.350
C(6)–C(7)	1.480(5)	1.470	1.467	1.469
C(7)–C(8)	1.421(4)	1.436	1.434	1.436
C(8)–C(9)	1.411(4)	1.413	1.408	1.412
C(9)–C(10)	1.467(4)	1.461	1.455	1.458

experimentally than the bond lengths calculated by the B3LYP method, especially in the case of the diruthenium complex. The results are shown in Table 5. Thus, the Ru–Ru bond distances obtained by the B1B95 and PBE1PBE methods are 2.878 and 2.902 Å, which are more close to the experimental data (2.866 Å) than the bond length calculated by the B3LYP method (2.971 Å). A similar tendency was observed for the average bond distances between Ru1 and carbons in the five-membered ring (η^5-bonding mode) and for those between Ru(2) and three carbons in the seven-membered ring (η^3-bonding mode); these are shown in Table 5 as italic. For the diiron complex, the Fe–Fe and Fe–C bond distances determined by crystallography are slightly shorter than those calculated by the B3LYP method, but slightly longer than those calculated by the B1B95 or PBE1PBE method; this seems to indicate that all three methods can be used for calculations of diiron complex. As representative examples, the molecular structures in the ground states for **3** and **4** calculated by the PBE1PBE method are illustrated in Fig. 5.

Studies on the potential energy surface were also performed by the B3LYP, B1B95 and PBE1PBE methods, and the transition state structures of the main pathway were determined. The representative bond distances calculated by the three methods are summarized in Table 6, and the transition state structures for the diiron and diruthenium complexes calculated by the PBE1PBE method are illustrated in Fig. 6. A transition state search from C_1 structures was carefully performed in the calculations with each functional, leading to the conclusion that there is only one transition state, which is C_s symmetric, during the haptotropic interconversion. In the transition state, there is a mirror plane including C(2), M(1), M(2), and C(7). The difference of the metal, *i.e.*, Ru or Fe, eventually affects the structure, in particular the metal–metal bond distance; that of **4** [Ru(1)–Ru(2); 2.851–2.929] is longer than that of **3** [Fe(1)–Fe(2); 2.642–2.768]. The metal–carbon distances between M(1) and the five-membered ring are also dependent on the metal; metal–carbon distances of **4** [Ru(1)–C_{Cp};

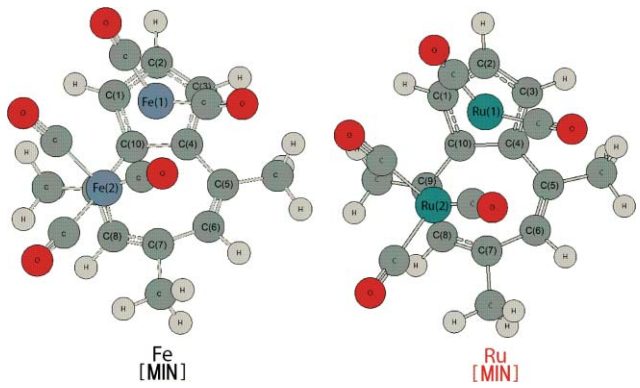

Fig. 5 Optimized ground state structures of **3** and **4** (PBE1PBE).

Table 6 Selected bond lengths (Å) for **3** and **4** by DFT calculation (transition state)

3 [Fe(TS)]			
	B3LYP	B1B95	PBE1PBE
Fe(1)–Fe(2)	2.768	2.662	2.642
Fe(1)–C(1)	2.137	2.087	2.088
Fe(1)–C(2)	2.113	2.066	2.079
Fe(1)–C(3)	2.137	2.087	2.088
Fe(1)–C(4)	2.158	2.104	2.114
Fe(1)–C(10)	2.158	2.104	2.114
Fe(1)–C_{η^5} (av.)	*2.141*	*2.090*	*2.097*
Fe(2)–C(6)	2.717	2.624	2.643
Fe(2)–C(7)	2.109	2.060	2.044
Fe(2)–C(8)	2.717	2.624	2.643
C(4)–C(5)	1.461	1.453	1.459
C(5)–C(6)	1.366	1.362	1.363
C(6)–C(7)	1.474	1.463	1.472
C(7)–C(8)	1.474	1.463	1.472
C(8)–C(9)	1.366	1.362	1.363
C(9)–C(10)	1.461	1.453	1.459
4 [Ru(TS)]			
	B3LYP	B1B95	PBE1PBE
Ru(1)–Ru(2)	2.929	2.851	2.862
Ru(1)–C(1)	2.338	2.271	2.283
Ru(1)–C(2)	2.350	2.281	2.291
Ru(1)–C(3)	2.338	2.271	2.283
Ru(1)–C(4)	2.339	2.267	2.283
Ru(1)–C(10)	2.339	2.267	2.283
Ru(1)–C_{η^5} (av.)	*2.341*	*2.271*	*2.285*
Ru(2)–C(6)	2.840	2.737	2.764
Ru(2)–C(7)	2.289	2.225	2.214
Ru(2)–C(8)	2.840	2.737	2.764
C(4)–C(5)	1.453	1.446	1.450
C(5)–C(6)	1.370	1.365	1.367
C(6)–C(7)	1.463	1.458	1.462
C(7)–C(8)	1.463	1.458	1.462
C(8)–C(9)	1.370	1.365	1.367
C(9)–C(10)	1.453	1.446	1.450

2.267–2.350 Å] are longer than **3** [Fe(1)–C_{Cp}; 2.066–2.158 Å]. The metal (M2)–carbon distances indicate that the C(7) atom is bonded with the metal [Fe(2)–C(7) 2.044–2.109 Å, Ru(2)–C(7) 2.214–2.289 Å]; however, M(2)–C(6) and M(2)–C(8) distances [Fe(2)–C(6) or Fe(2)–C(8) 2.623–2.717 Å, and Ru(2)–C(6) or Ru(2)–C(8) 2.737–2.840 Å] are longer than M(2)–C(7) by 0.6 Å, suggesting no metal–carbon interaction. In other words, the coordination mode of the transition state **X** is μ_2,η^1,η^5, being coordinatively unsaturated. Thus, the rearrangement takes place by slipping the metal carbonyl species on the conjugated π-electrons through a coordinatively unsaturated transition state; this is similar to the rearrangement of (η^6-naphthalene)$Cr(CO)_3$.

A notable feature of the transition state structures is that shorter metal–metal and metal–carbon distances of the diiron complexes provide substantial deviation of the azulene ligand leading to the distorted transition state structure as shown in Fig. 6 (bottom) and Table 7 (*e.g.* for PBE1PBE method; $\theta = 21°$, $\phi = 53°$). In contrast, the longer Ru–Ru distance retains the planarity of the azulene ligand (*e.g.* for PBE1PBE method; $\theta = 17°$, $\phi = 42°$) at the transition state. This may provide one explanation for the $\Delta S^{\ddagger}$ (Fe) < $\Delta S^{\ddagger}$ (Ru) observed in the kinetic and SST experiments of the diiron complexes **1** and **3**. A smaller $\Delta S^{\ddagger}$ is generally explained by a decrease in freedom of motions from the ground state to transition state. One plausible explanation of $\Delta S^{\ddagger}$ (Fe) < $\Delta S^{\ddagger}$ (Ru) may be related to the decrease of planarity of the azulene ligand in the diiron complex at the transition state, which causes loss of the motion of freedom of this ligand. Estimation of thermodynamic parameters from the DFT calculations may provide some information on the question of experimentally observed features of $\Delta S^{\ddagger}$. Although the $\Delta G^{\ddagger}$ and $\Delta S^{\ddagger}$ values estimated from the theoretical calculations are roughly parallel to the experimental results, the $\Delta H^{\ddagger}$ from the DFT calculations is not consistent with that experimentally determined as summarized in

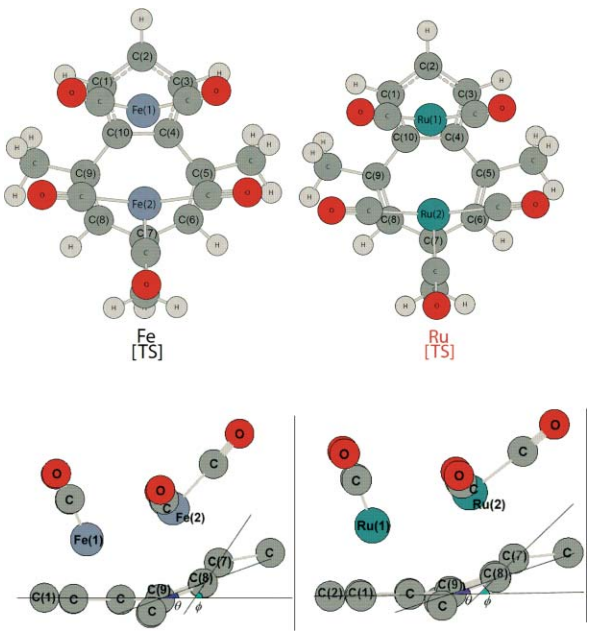

Fig. 6 The transition state structures of **3** and **4** [top and side views] (PBE1PBE method).

Table 7 Dihedral angles of planes defined by θ and ϕ in Fig. 6

	3			**4**		
	B1B95	B3LYP	PBE1PBE	B1B95	B3LYP	PBE1PBE
θ	21	21	21	16	16	17
ϕ	50	51	53	39	41	42

the ESI.†[19] Detailed discussion on the thermodynamic parameters should be awaited for further theoretical studies.

Conclusions

As described above, the results in this paper revealed the haptotropic rearrangement of (μ_2,η^3:η^5-4,6,8-trimethylazulene)-$Fe_2(CO)_5$ (**3**) and (μ_2,η^3:η^5-4,6,8-trimethylazulene)$Ru_2(CO)_5$ (**4**) by the SST technique of ^{1}H NMR and DFT calculation with the B3LYP, B1B95 and PBE1PBE methods. The SST method provided entropy, enthalpy and Gibbs energy of rearrangement, which are comparable to those for the guaiazulene homologues, **1** and **2**. The DFT calculations, in particular, the PBE1PBE method showed the optimized structures for **3** and **4** are very similar to those determined by crystallography. The search for the transition states indicated a simple slippage of the M_2 fragment on the azulene ligand while keeping the M–M bond intact for both the haptotropic rearrangement of **3** and **4**. The larger deviation from planarity of the azulene ligand in the diiron complex than that in the diruthenium complex is suggested from the calculated transition state structures, which may explain the $\Delta S^{\ddagger}$ (Fe) > $\Delta S^{\ddagger}$ (Ru) observed experimentally. These results clearly demonstrate that combination of the SST method as well as DFT calculations successfully analyzes the haptotropic rearrangement of dinuclear metal carbonyls bound to conjugated π-ligands; we expect that these methods are useful for the rearrangements in the solid state and those of the dinuclear complexes having conjugate π-ligands other than azulenes with similar approaches. From the standpoint of application of the DFT calculations to the analysis of the organometallic reactions, it is noteworthy that use of one-parameterized hybrid functions, B1B95 and PBE1PBE, provided the bond distances of the optimized ground state structures better fitting to the experimental data, especially for the diruthenium complex. Although the B3LYP method is commonly used for the calculations of organometallic reactions at present, the present results apparently indicates that the B1B95 and PBE1PBE methods sometimes provide better results than the B3LYP method.

Experimental

General

All experiments were carried out under an argon atmosphere using standard Schlenk techniques. All of the solvents were distilled in the presence of standard drying reagents just before use. 4,6,8-Trimethylazulene was synthesized according to a procedure in the literature.[20] The ^{1}H and ^{13}C NMR spectra were taken with a JEOL ECA 400 or 600 spectrometer. Chemical shifts were recorded in ppm from the residual peaks of the solvent and proton assignments are on the basis of Fig. 7. IR spectra were recorded in cm^{-1} on a JASCO FT/IR-550 spectrometer. Elemental analyses were carried out by the Center of Elementary Analysis, Kyushu University.

Synthesis of (μ_2,η^3:η^5-4,6,8-trimethylazulene)$Fe_2(CO)_5$ (3). A xylene solution (25 mL) of 4,6,8-trimethylazulene (300 mg, 1.76 mmol) and an excess amount of $Fe(CO)_5$ (5 mL, 38 mmol) was heated under reflux with stirring for 2 days. After concentration of the reaction mixture, the residue was purified by silica gel column chromatography eluting with hexane. The combined brown eluents were concentrated, and the resulting oversaturated solution was cooled at −30 °C. Brown block crystals of (μ_2,η^3:η^5-4,6,8-trimethylazulene)$Fe_2(CO)_5$ were formed from the solution, which were collected and dried *in vacuo.* (37% yield). Brown block crystals; mp 120 °C (decomp.). ^{1}H NMR (xylene-d_{10}, 600 MHz, r.t.) δ 4.81 (s, 1H (H7)), 4.48 (s, 1H (H5)), 4.44 (dd, J = 2.7, 2.0 Hz, 1H (H1)), 4.37 (t, J = 2.7 Hz, 1H (H2)), 3.16 (dd, J = 2.7, 2.0 Hz, 1H (H3)), 1.59 (s, 3H (Me)), 1.48 (s, 3H (Me)), 1.26 (s, 3H (Me)). ^{13}C NMR (xylene-d_{10}, 151 MHz, r.t.) δ 20.9, 23.9, 30.3, 67.0, 71.2, 76.6, 81.9, 82.1, 82.7, 84.4, 87.7, 125.9, 131.4; carbonyl region 214.9, 216.5, 219.8. ^{1}H NMR (CD_2Cl_2, 600 MHz, −50 °C) δ 5.25 (dd, J = 2.7, 2.0 Hz, 1H (H1)), 5.22 (dq, J = 1.2, 1.2 Hz, 1H (H5)), 5.16 (dd, J = 2.7, 2.7 Hz, 1H (H2)), 5.13 (s, 1H (H7)), 3.92 (dd, J = 2.7, 2.0 Hz, 1H (H3)), 2.11 (s, 3H (Me)), 1.77 (s, 3H (Me)), 1.63 (d, J = 1.2 Hz, 3H (Me)). ^{13}C NMR (CD_2Cl_2, 151 MHz, −50 °C) δ 21.0, 24.2, 30.2, 67.7, 71.3, 76.8, 81.5, 82.3, 83.2, 84.3, 87.5, 125.9, 130.7; carbonyl region 215.3, 217.1, 220.5, 221.3, 221.4. IR (KBr, cm^{-1}) ν(CO): 2022, 1973, 1957, 1932 cm^{-1}. Anal. Calcd for $C_{18}H_{14}O_5Fe_2$: C, 51.23; H, 3.34. Found: C, 51.27; H, 3.42%.

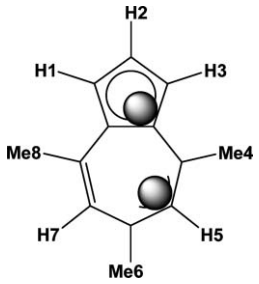

Fig. 7 Proton assignments of complexes **3** and **4**.

Synthesis of (μ_2,η^3:η^5-4,6,8-trimethylazulene)$Ru_2(CO)_5$ (4). A heptane solution (50 mL) of 4,6,8-trimethylazulene (299 mg, 1.76 mmol) and $Ru_3(CO)_{12}$ (565 mg, 0.884 mmol) was heated under reflux with stirring for 5 h to form a mixture of **4**, (μ_2,η^3:η^5-4,6,8-trimethylazulene)$Ru_3(CO)_7$, and (μ_2,η^3:η^5-4,6,8-trimethylazulene)$Ru_4(CO)_9$, from which **4** was isolated by silica gel column chromatography eluting with CH_2Cl_2/hexane. The first band containing **4** and the solvent was removed from the eluents to give (μ_2,η^3:η^5-4,6,8-trimethylazulene)$Ru_2(CO)_5$ (129 mg, 25% yield). Yellow block crystals, mp 122 °C (decomp.). ^{1}H NMR (xylene-d_{10}, 600 MHz, r.t.) δ 5.05 (dd, J = 2.9, 2.1 Hz, 1H (H1)), 4.96 (t, J = 2.9 Hz, 1H (H2)), 4.61 (s, 1H (H7)), 4.47 (dq, J = 1.2, 1.2 Hz, 1H (H5)), 3.21 (dd, J = 2.9, 2.1 Hz, 1H (H3)), 1.57 (s, 3H, Me), 1.55 (s, 3H, Me), 1.21 (d, J = 1.2 Hz, 3H (Me)). ^{13}C NMR (xylene-d_{10}, 151 MHz, r.t.) δ 24.6, 30.5, 32.1, 63.4, 65.8, 78.4, 82.8, 84.1, 86.8, 89.3, 116.7, 123.2, 129.2; carbonyl region 203.5, 208.9. ^{1}H NMR (CD_2Cl_2, 600 MHz, −50 °C) δ 5.77 (dd, J = 3.0, 2.0 Hz, 1H (H1)), 5.67 (dd, J = 3.0, 3.0 Hz, 1H (H2)), 5.29 (s, 1H (H7)), 4.83 (dq, J = 1.2, 1.2 Hz, 1H (H5)), 3.97 (dd, J = 2.9, 2.1 Hz, 1H (H3)), 2.10 (s, 3H (Me)), 1.86 (s, 3H (Me)), 1.53 (d, J = 1.2 Hz, 3H (Me)). ^{13}C NMR (CD_2Cl_2, 151 MHz, −50 °C) δ 20.6, 24.9, 31.9, 63.1, 66.5, 78.5, 83.2, 84.4, 86.6, 86.8, 88.5, 123.0, 128.9; carbonyl region 203.9, 206.4, 206.5, 209.6, 210.3. IR (KBr, cm^{-1}) ν(CO): 2045, 1989, 1971, 1914 cm^{-1}. Anal. Calcd for $C_{18}H_{14}O_5Ru_2$: C, 42.18; H, 2.75. Found: C, 42.19; H, 2.76%.

Spin-saturation transfer measurements

All the SST studies were carried out with the JEOL ECA 600 MHz NMR instrument, for which probe temperatures were calibrated externally using measurements of ethylene glycol at each temperature. We checked several deuterated solvents for the SST measurements, and found that xylene-d_{10} was the most suitable among them. In this solvent, peak separation is adequate at a temperature range from 80 to 140 °C. A solution of the complex was placed in a 5-mm diameter NMR tube which was degassed several times and the tube was sealed in a flame, while the solution was kept in a dry-ice acetone bath in vacuum. The spin–lattice relaxation times were measured by the inversion recovery method as the average of ten measurements. The spin saturation and the transfer of the resulting saturated spin from H3 to H1 were carried out by irradiation of H3 for a period of $>5T_1$, which is sufficient to equilibrate the haptotropic isomerization and the spin relaxation, before the NMR measurement. The decreased intensity of H1 was calculated by comparison of its integral value with the other peak which was not affected by the SST measurements. The data reported in Table 3 are the average of ten measurements. The rate constant k was calculated according to the method described in the text, and the Eyring plot of k at six different temperatures provided the thermodynamic parameters using eqn (2):

$$\ln\left(\frac{k}{T}\right) = \ln\left(\frac{k_B}{T}\right) - \frac{\Delta H}{RT} + \frac{\Delta S}{R} \quad (2)$$

Methods of calculations

All geometrical optimizations were carried out using B3LYP, B1B95 and PBE1PBE methods. The B3LYP method is the hybrid density functional theory with the Becke three-parameterized correlation functional and the Lee–Yang–Parr exchange–correlation functional.[13] B1B95 has been implemented by Adamo and Barone, and PBE1PBE is the 1997 hybrid functional of Perdew, Burke and Ernzerhof. The ratios between Hartree–Fock and density functional exchange on these B1B95 and PBE1PBE functionals are determined *a priori* from purely theoretical considerations and no further parameters are present. These one-parameterized functionals give excellent thermochemistry in the G2 benchmarks of Pople *et al*.[21] The triple-zeta valence GTO basis set with Effective Core potential was used for Fe and Ru which was developed by Stevens, Basch and Krauss (CEP-31G).[14] Dunning's correlation consistent basis sets of double-zeta type cc-pVDZ[15] were used for C, O, and H. All calculations were performed using the GAUSSIAN-98 program.[22] Vibrational analyses were performed for each optimized structure, and the numbers of imaginary frequencies (negative signs) for each structure help us to determine the curvature on the potential surface. The thermodynamic parameters were also estimated by using these vibrational analyses. The technical details for the calculation of thermodynamic parameters are reviewed in ref. 23.

X-Ray data collection and reduction

X-Ray crystallography was performed on a Rigaku Saturn CCD area detector with graphite monochromated Mo-Kα radiation ($\lambda = 0.71070$ Å). The reflection data were collected at 123(2) K using ω scans in the θ range of 3.1–27.5 for **3** and 3.3–27.5 for **4**. The data obtained were processed using Crystal-Clear (Rigaku) on a Pentium computer, and were corrected for Lorentz and polarization effects. The structures were solved by direct methods (SIR92)[24] and expanded using Fourier techniques.[25] The non-hydrogen atoms were refined anisotropically, and the hydrogen atoms were placed using the riding model. The final cycle of full-matrix least-squares refinement on F^2 was based on 3720 observed reflections and 240 variable parameters for **3**, and on 3944 observed reflections and 240 variable parameters for **4**. Neutral atom scattering factors were taken from Cromer and Waber.[26] All calculations were performed using the CrystalStructure[27,28] crystallographic software package. Details of the final refinement are summarized in Table 1, and the numbering scheme employed is shown in Fig. 1, which was drawn with ORTEP at 50% probability ellipsoids.

Acknowledgements

This work was supported by Grant-in-Aid for Scientific Research on Priority Areas (No. 14078101, "Reaction Control of Dynamic Complexes") from Ministry of Education, Culture, Sports, Science and Technology, Japan.

Notes and references

1 (*a*) For a review: J. O'Connor and C. P. Casey, *Chem. Rev.*, 1987, **87**, 307; (*b*) a general introduction: J. P. Collman, L. S. Hegedus, J. R. Norton, R. G. Finke, *Principles and Applications of Organotransition Metal Chemistry*, University Science Books, Mill Valley, CA, 1987.
2 (*a*) B. E. Mann, in *Comprehensive Organometallic Chemistry*, ed. G. Wilkinson, F. G. A. Stone and E. W. Abel, Pergamon, Oxford, 1982, vol. 3, ch. 20; (*b*) B. E. Mann, *Chem. Soc. Rev.*, 1986, **15**, 167.
3 G. Degenello, *Transition Metal Complexes of Cyclic Polyolefins*, Academic Press, London, 1982.
4 (*a*) P. M. Treichel and J. W. Johnson, *Inorg. Chem.*, 1977, **16**, 749; (*b*) R. U. Kirss and P. M. Treichel, *J. Am. Chem. Soc.*, 1986, **108**, 853; (*c*) M. E. Rerek and F. Basolo, *Organometallics*, 1984, **3**, 647; (*d*) N. A. Ustynyuk, L. N. Novikova, Y. F. Oprunenko, S. G. Malyugina and Y. A. Ustynyuk, *J. Organomet. Chem.*, 1984, **277**, 75; (*e*) K. Nakasuji, M. Yamaguchi and I. Murata, *J. Am. Chem. Soc.*, 1986, **108**, 325; (*f*) Y. Oprunenko, S. Malyugina, A. Vasil'ko, K. Lyssenko, C. Elschenbroich and K. Harms, *J. Organomet. Chem.*, 2002, **641**, 208.
5 (*a*) J. Silvestre and T. A. Albright, *J. Am. Chem. Soc.*, 1985, **107**, 6829; (*b*) T. A. Albright, P. Hofmann, R. Hoffmann, C. P. Lillya and P. A. Dobosh, *J. Am. Chem. Soc.*, 1983, **105**, 3396; (*c*) L. F. Veiros, *J. Organomet. Chem.*, 1999, **587**, 221.
6 (*a*) O. I. Trifonova, E. A. Ochertyanova, N. G. Akhmedov, V. A. Roznyatovsky, D. N. Laikov, N. A. Ustynyuk and Y. A. Ustynyuk, *Inorg. Chim. Acta.*, 1998, **280**, 328; (*b*) Y. F. Oprunenko, N. G. Akhmedov, D. N. Laikov, S. G. Malyugina, V. I. Mstislavsky, V. A. Roznyatovsky, Y. A. Ustynyuk and N. A. Ustynyuk, *J. Organomet. Chem.*, 1999, **583**, 136.
7 (*a*) F. A. Cotton, B. E. Hanson, J. R. Kolb, P. Lahuerta, G. G. Stanley, B. R. Stults and A. J. White, *J. Am. Chem. Soc.*, 1977, **99**, 3673; (*b*) H. Nagashima, T. Fukahori, M. Nobata, A. Suzuki, M. Nakazawa and K. Itoh, *Organometallics*, 1994, **13**, 3427; (*c*) K. Matsubara, T. Oda and H. Nagashima, *Organometallics*, 2001, **20**, 881; (*d*) K. Matsubara, S. Mima, T. Oda and H. Nagashima, *J. Organomet. Chem.*, 2002, **650**, 96.
8 (*a*) H. Nagashima, T. Fukahori and K. Itoh, *J. Chem. Soc. Chem. Commun.*, 1991, 786; (*b*) S. Niibayashi, K. Matsubara, M. Haga and H. Nagashima, *Organometallics*, 2004, **23**, 635.
9 (*a*) F. A. Cotton, D. L. Hunter and P. Lahuerta, *J. Am. Chem. Soc.*, 1975, **97**, 1046; (*b*) F. A. Cotton and D. L. Hunter, *J. Am. Chem. Soc*, 1975, **97**, 5739; (*c*) M. D. Fryzuk, L. Jafarpour, F. M. Kerton, J. B. Love and S. J. Rettig, *Angew. Chem., Int. Ed.*, 2000, **39**, 767; (*d*) M. D. Fryzuk, J. B. Love and S. J. Rettig, *J. Am. Chem. Soc.*, 1997, **119**, 9071; (*e*) M. D. Fryzuk, L. Jafarpour, F. M. Kerton, J. B. Love, B. O. Patrick and S. J. Rettig, *Organometallics*, 2001, **20**, 1387.

10 (*a*) J. W. Faller, *Determination of Organic Structures by Physical Methods*, ed. F. C. Nachod and J. J. Zuckerman, Academic Press, New York, 1973, vol. 5, ch. 2; (*b*) J. Sandstrom, *Dynamic NMR Spectroscopy*, Academic, New York, 1982; (*c*) A. E. Derome, *Modern NMR Techniques for Chemistry Research*, Pergamon, Oxford, 1987; (*d*) R. L. Jarek, R. J. Flesher and S. K. Shin, *J. Chem. Educ.*, 1997, **74**, 978.

11 (*a*) For applications to SST to the haptotropic rearrangement: K. J. Karel and M. Brookhart, *J. Am. Chem. Soc.*, 1978, **100**, 1619; (*b*) Z. Goldschmidt and H. E. Gottlieb, *J. Organomet. Chem.*, 1989, **361**, 207; (*c*) A. Stanger, *Organometallics*, 1991, **10**, 2979; (*d*) A. Stanger and H. Weismann, *J. Organomet. Chem.*, 1996, **515**, 183.

12 H. Nagashima, A. Suzuki, M. Nobata, K. Aoki and K. Itoh, *Bull. Chem. Soc. Jpn.*, 1998, **71**, 2441.

13 (*a*) A. D. Becke, *J. Chem. Phys.* 1993, 98, 5648; (*b*) R. G. Parr, W. Yang, *Density-Functional Theory of Atoms and Molecules*, Oxford University Press, Inc., New York, 1989.

14 (*a*) T. R. Cundari and W. J. Stevens, *J. Chem. Phys.*, 1993, **98**, 5555; (*b*) W. J. Stevens, H. Basch and M. Krauss, *J. Chem. Phys.*, 1984, **81**, 6026.

15 D. E. Woon and T. H. Dunning Jr., *J. Chem. Phys.*, 1993, **98**, 1358.

16 (*a*) W. Koch and M. C. Holthausen, *A Chemist's Guide to Density Functional Theory*, Wiley-VCH, 2nd edn, 2000; (*b*) P. E. M. Siegbahn, *Adv. Chem. Phys.*, 2000, **93**, 333–338.

17 (*a*) D. Becke, *J. Chem. Phys.*, 1996, **104**, 1040; (*b*) C. Adamo and V. Barone, *Chem. Phys. Lett.*, 1997, **274**, 242.

18 (*a*) J. P. Perdew, K. Burke and M. Ernzerhof, *Phys. Rev. Lett.*, 1996, **77**, 3865; (*b*) J. P. Perdew, K. Burke and M. Ernzerhof, *Phys. Rev. Lett.*, 1997, **78**, 1396.

19 Oprunenko *et al*. reported in their DFT calculations of the haptotropic rearrangement of (η^6-naphthalene)$Cr(CO)_3$, in which 'Considering the inherent approximations (approximation of isolated molecule, neglecting the difference of energies of zero vibration) the calculated activation barriers are in a good accordance with the experimentally determined $\Delta G^{\ddagger}$ values.'[6b] In our calculations, too, calculated E is from 19 to 27 kcal mol^{-1}, which is roughly parallel to the experimentally determined $\Delta G^{\ddagger}$. However, the large difference in $\Delta H^{\ddagger}$ was determined by our DFT calculations as summarized in the ESI†.

20 M. E. Garst, J. Hochlowski, J. G. Douglass III and S. Sasse, *J. Chem. Educ.*, 1983, **60**, 510.

21 (*a*) J. A. Pople, M. Head-Gordon, D. J. Fox, K. Raghavachari and L. A. Curtiss, *J. Chem. Phys.*, 1989, **90**, 5622; (*b*) L. A. Curtiss, C. Jones, G. W. Trucks, K. Raghavachari and J. A. Pople, *J. Chem. Phys.*, 1990, **93**, 2537; (*c*) L. A. Curtiss, K. Raghavachari, G. W. Trucks and J. A. Pople, *J. Chem. Phys.*, 1991, **94**, 7221; (*d*) P. M. W. Gill, B. G. Johnson, J. A. Pople and M. J. Frisch, *Int. J. Quantum Chem. Quantum Chem. Symp.*, 1992, **26**, 319.

22 Gaussian 03, Revision B.04, M. J. Frisch, G. W. Trucks, H. B. Schlegel, G. E. Scuseria, M. A. Robb, J. R. Cheeseman, J. A. Montgomery Jr., T. Vreven, K. N. Kudin, J. C. Burant, J. M. Millam, S. S. Iyengar, J. Tomasi, V. Barone, B. Mennucci, M. Cossi, G. Scalmani, N. Rega, G. A. Petersson, H. Nakatsuji, M. Hada, M. Ehara, K. Toyota, R. Fukuda, J. Hasegawa, M. Ishida, T. Nakajima, Y. Honda, O. Kitao, H. Nakai, M. Klene, X. Li, J. E. Knox, H. P. Hratchian, J. B. Cross, C. Adamo, J. Jaramillo, R. Gomperts, R. E. Stratmann, O. Yazyev, A. J. Austin, R. Cammi, C. Pomelli, J. W. Ochterski, P. Y. Ayala, K. Morokuma, G. A. Voth, P. Salvador, J. J. Dannenberg, V. G. Zakrzewski, S. Dapprich, A. D. Daniels, M. C. Strain, O. Farkas, D. K. Malick, A. D. Rabuck, K. Raghavachari, J. B. Foresman, J. V. Ortiz, Q. Cui, A. G. Baboul, S. Clifford, J. Cioslowski, B. B. Stefanov, G. Liu, A. Liashenko, P. Piskorz, I. Komaromi, R. L. Martin, D. J. Fox, T. Keith, M. A. Al-Laham, C. Y. Peng, A. Nanayakkara, M. Challacombe, P. M. W. Gill, B. Johnson, W. Chen, M. W. Wong, C. Gonzalez, J. A. Pople, Gaussian, Inc., Pittsburgh PA, 2003.

23 J. W. Ochterski, *Thermochemistry in Gaussian*, 2000; http://www.gaussian.com.

24 A. Altomare, M. C. Burla, M. Camalli, G. Cascarano, C. Giacovazzo, A. Guagliardi and G. Polidori, *J. Appl. Crystallogr.*, 1994, **27**, 435.

25 P. T. Beurskens, G. Beurskens, R. de Gelder, S. Garcia-Granda, R. O. Gould, R. Israel and Jan M. M. Smits, *The DIRDIF-99 program system*, Crystallography Laboratory, University of Nijmegen, The Netherlands, 1998.

26 D. T. Cromer and J. T. Waber, *International Tables for X-ray Crystallography*, Kynoch Press, Birmingham, UK, 1974, vol. 4.

27 Crystal Structure 3.8: Crystal Structure Analysis Package; Package, Rigaku and Rigaku/MSC, 9009 New Trails Dr., The Woodlands, TX 77381, USA, 2000–2006.

28 *CRYSTALS Issue 11*: J. R. Carruthers, J. S. Rollett, P. W. Betteridge, D. Kinna, L. Pearce, A. Larsen and E. Gabe, Chemical Crystallography Laboratory, Oxford, UK, 1999.

